Encapsulation of manganese dioxide nanoparticles into layer-by-layer polymer capsules for the fabrication of antioxidant microreactors

Encapsulation of manganese dioxide nanoparticles into layer-by-layer polymer capsules for the fabrication of antioxidant microreactors

E. Marin[a], C. Tapeinos[b], S. Lauciello[c], G. Ciofani[b], J. R. Sarasua[a], A. Larrañaga[a,*]

[a] University of the Basque Country (UPV/EHU), Department of Mining-Metallurgy Engineering and Materials Science & POLYMAT, Faculty of Engineering in Bilbao, Plaza Torres Quevedo 1, 48013 Bilbao, Spain.
[b] Italian Institute of Technology (IIT), Smart Bio-Interfaces, Viale Rinaldo Piaggio 34, 56025 Pontedera, Italy.
[c] Italian Institute of Technology (IIT), Electron Microscopy Facility, Via Morego 30, Genova, Italy.
* Corresponding author. Phone: +0034 946 013935. E-mail: aitor.larranagae@ehu.eus

Abstract

Oxidative stress is caused by the accumulation of reactive oxygen and nitrogen species (ROS and RNS) in the cellular microenvironment. These ROS and RNS damage important cell structures leading to cell apoptosis and senescence, thus causing a detrimental effect on numerous disease pathologies such as osteoarthritis, neurodegeneration and cardiovascular diseases. For this reason, there is a growing interest in the development of antioxidant biomaterials that can eventually regulate the levels of ROS/RNS and prevent oxidative stress. The encapsulation of antioxidant enzymes (e.g., catalase or superoxide dismutase) on polymer microcapsules fabricated via the layer-by-layer (LbL) approach represents a promising strategy within this context. The diffusion of reagents and by-products through the shell of these microcapsules is timely and spatially controlled, allowing the bio-chemical reaction between ROS/RNS and the encapsulated enzyme. However, natural enzymes usually present low stability, high cost and difficult storage, which could limit their potential application in the biomedical field. Hence, nanomaterials with intrinsic enzyme-like characteristics (i.e., nanozymes) have been considered as inorganic alternatives. In the present work, manganese dioxide nanoparticles were encapsulated into LbL polymer microcapsules to yield synthetic antioxidant microreactors. These microreactors efficiently scavenged hydrogen peroxide (H_2O_2) from solution and protected cells from oxidative stress in an *in vitro* model. The versatility of the synthetic procedure presented herein allows the fabrication of capsules with either positive or negative surface charge, which has a direct impact on the cytotoxicity and cell interaction. This study represents accordingly a novel strategy to obtain antioxidant polymer microreactors based on synthetic (nano)materials for the treatment of oxidative stress.

Keywords: Oxidative stress; polymer capsules; manganese dioxide; layer-by-layer; antioxidant activity.

1. Introduction

Reactive oxygen species (ROS) such as hydrogen peroxide (H_2O_2), hydroxyl (·OH) and superoxide anion radicals (O_2^-) are reactive molecules which play an essential role in numerous cell signalling processes [1]. In normal cellular activity conditions, cells are capable of regulating efficiently the levels of ROS through several antioxidant enzymes and molecules. However, an overproduction of these ROS can overwhelm the antioxidant capacity of the cells and induce oxidative stress, which is the cause of numerous pathologies like neurodegeneration, cancer, osteoarthritis and cardiovascular diseases [1–4].

For the reduction of the overproduced ROS, different alternatives based on biomaterials have been widely studied, including polymer micro- and nanocapsules fabricated via the layer-by-layer (LbL) approach. These consist on the alternate deposition of oppositely charged polyelectrolytes on a colloidal template, which is subsequently removed [5]. This process allows the fabrication of tailor-made micro- and nanocapsules with the possibility to adapt their physical, chemical, morphological and mechanical properties to the required application [6,7]. More precisely, the thickness of the polymeric membrane and the amount of polyelectrolyte attached to the sacrificial template can be tuned changing the polymerization degree of the polyelectrolytes, adjusting the ionic strength of the polyelectrolyte solution or modulating the template-polyelectrolyte amount ratio to ensure an efficient layer adhesion [8]. To impart advanced functionalities to the fabricated polymer micro- and nanocapsules, the outer layer can be chemically functionalized with several biomolecules [9]. Alternatively, inorganic nanoparticles can be incorporated either within the capsule or between the layers to create stimulus-responsive micro- and nanocapsules [10–13].

Thanks to the versatility of this process, the fabricated capsules have been used for different biomedical applications such as drug delivery vehicles [14–16], imaging [17,18], or, more recently, as micro- and nanoreactors [19,20]. In the latter case, the capsules accommodate within their core active biomolecules such as enzymes, which act *in situ* allowing the continuous transfer of reagents and products through the polymeric membrane. Enzymes like catalase [19] or superoxide dismutase (SOD) have been widely studied for the reduction of the overproduced ROS. However, the exposure of these enzymes to diverse environmental conditions (e.g., extreme pH, high temperature, organic solvent) have a detrimental effect on their catalytic activity, thus limiting their practical application [21].

As an inorganic alternative to these antioxidant enzymes, nanozymes (e.g., CeO_2 [20,22] or MnO_2 [1,23–25]) have gained interest in nanobiotechnology owing to their high catalytic efficiency and robust stability [21,23,26,27]. Manganese dioxide nanoparticles are of particular interest as ROS scavengers because of their multienzyme nature that mimic simultaneously the activity of both catalase and SOD [23]. Furthermore, the decomposition of these nanoparticles in Mn^{2+} and H_2O, preventing their accumulation in the body, makes manganese dioxide a good inorganic alternative for the treatment of oxidative stress [1].

In this study, it was hypothesized that MnO_2-loaded polymer microcapsules would protect cells from H_2O_2-induced oxidative stress. We fabricated polymer capsules loaded with MnO_2 nanoparticles via the LbL process, depositing alternately poly(sodium 4-styrenesulfonate) (PSS) and poly(allylamine hydrochloride) (PAH) on a MnO_2-decorated $CaCO_3$ sacrificial template. After the $CaCO_3$ template removal, antioxidant polymer capsules loaded with MnO_2 nanoparticles were obtained. The capsules were thoroughly characterized in terms of physico-chemical, morphological and functional properties and, as a proof of concept, their therapeutic

potential was evaluated in a preliminary *in vitro* model of oxidative stress using HeLa cells. This study represents accordingly a significant advance in the development and therapeutic application of antioxidant microreactors for the treatment of oxidative stress.

2. Materials and methods

2.1. Materials

Calcium chloride ($CaCl_2$), sodium carbonate (Na_2CO_3), sodium chloride (NaCl), potassium permanganate ($KMnO_4$), hydrogen peroxide (H_2O_2) (30% wt. in H_2O), poly(allylamine hydrochloride) (PAH) (M_w ~ 17,500 g/mol), poly(sodium 4-styrenesulfonate) (PSS) (M_w ~ 70,000 g/mol), ethylenediaminetetraacetic acid disodium salt dihydrate (EDTA), fluorescein 5-isothiocyanate (FITC), Phosphate Buffer Saline (PBS), Hank's Balanced Salt Solution (HBSS), Triton X-100, Tween 20 and bovine serum albumin (BSA) were purchased from Sigma Aldrich. Dulbecco's modified Eagle's medium (DMEM), fetal bovine serum (FBS), penicillin-streptomycin solution (P/S), AlamarBlue® cell viability reagent, rhodamine-phalloidin, 4',6-diamidino-2-phenylindole dihydrochloride (DAPI) and 16% Formaldehyde Solution (w/v) were purchased from Thermo Fischer Scientific.

2.2. Synthesis and characterization of MnO_2 nanoparticles

2.2.1. Synthesis of MnO_2 nanoparticles

MnO_2 nanoparticles were synthesized using a modified procedure as previously reported [1,3,28]. Briefly, 27.5 mM of $KMnO_4$ was dissolved in 150 mL of distilled water inside a conical flask, and left under stirring (300 rpm) for 15 min. In parallel and in a smaller conical flask, 1.1 mM of PAH was dissolved in 50 mL of distilled water and stirred (300 rpm) again

for 15 min. After 15 min, the stirring speed of the $KMnO_4$ solution was increased at 600 rpm and the aqueous solution of PAH was added. The mixed solution was stirred for 24 h and then freeze dried for 48-96 h. The freeze-dried sample was resuspended in 10 mL of distilled water inside a 15 mL falcon tube with the help of an ultrasonic probe (90 % amplification for 5 min), and then was washed 3 times by centrifugation at 7000 g. After each centrifugation, the precipitate was redispersed in distilled water either by shaking or vortexing. After the third spinning, the precipitate was dispersed in distilled water using an ultrasonic probe for 1 h (90% amplification) inside an ice bath. The dispersion was kept at 4 °C until further use.

2.2.2. Characterization of MnO_2 nanoparticles

The morphological analysis of the MnO_2 nanoparticles was carried out by means of Scanning Electron Microscopy (SEM: FEI 200) at a working voltage and working current of 10 kV and 43 pA, respectively and by Transmission Electron Microscopy (TEM: JEM 1011, Jeol, Tokyo, Japan) at an accelerating voltage of 100 keV. The samples for the TEM were prepared by drop-casting 6 µl of solution previously diluted onto ultrathin C-film 150 mesh Cu grids.

Fourier-transform infrared spectroscopy (FTIR) was performed using a Shimadzu Miracle 10. The number of scans was set to 45, the scanning range was set from 4000 to 400 cm^{-1} and the resolution step at 4 cm^{-1}.

The size distribution as well as the surface charge were measured using a Zetasizer NanoZS90, Malvern instruments LTD. The measurements were carried out at 25 °C in distilled water at a concentration of 200 µg/mL. The size and the surface charge measurements represent the mean ± SD of three different measurements, with ten runs of ten seconds for each measurement.

Before each measurement, the samples were sonicated for ten seconds using a Bandelin ultrasonic probe at 8 W, to avoid the presence of aggregates during measurements.

2.3. Fabrication and characterization polymer capsules

2.3.1. Fabrication of polymer capsules

Polymer capsules were fabricated via the LbL process using $CaCO_3$ microparticles as a sacrificial template and PSS and PAH as negative and positive polyelectrolytes, respectively. $CaCO_3$ particles stabilized with PSS were obtained by the fast precipitation reaction between $CaCl_2$ and Na_2CO_3, similar to previous reports [29]. Briefly, aqueous solutions of 0.2 M $CaCl_2$ and Na_2CO_3 were prepared separately. 0.2 M Na_2CO_3 solution was prepared in the presence of PSS (4 mg/mL). The $CaCl_2$ solution was quickly poured into the PSS-Na_2CO_3 solution in an equal volume. After 30 s of vigorous stirring, the solution was incubated for 15 min. The obtained dispersion was centrifuged at 2000 g (1 min) and the particles were washed 3 times with distilled water. Then the particles were resuspended in a 4 mg/mL MnO_2 aqueous solution (4 mg MnO_2 nanoparticles:10 mg $CaCO_3$ microparticles) and incubated in an orbital shaker at 300 rpm (30 min). After the incubation, the dispersion of particles was washed three times with a 0.005 M NaCl solution to remove the excess of MnO_2 nanoparticles. The amount of adsorbed MnO_2 nanoparticles onto the $CaCO_3$ templates was assessed by dissolving the template in a 0.1 M EDTA solution. First, a calibration curve of MnO_2 in a 0.1 M EDTA solution was prepared. $CaCO_3$ templates were incubated with different concentrations of MnO_2 nanoparticles and after the washing steps described above, templates were immersed in the EDTA solution thrice. The supernatant of each incubation step was collected and the MnO_2 concentration was determined by UV-VIS (Perkin Elmer lambda 365) at λ = 385 nm. Thereafter, the particles were

resuspended in a 2 mg/mL PSS solution in 0.5 M NaCl (pH 6.5) and after ten minutes of incubation, the particles were centrifuged and washed thrice with a 0.005 M NaCl solution. After that, the particles were resuspended in a 2 mg/mL PAH solution in 0.5 M NaCl (pH 6.5) and incubated for ten minutes. This process was repeated until the desired number of layers was deposited. Finally, the particles were immersed in a 0.1 M EDTA solution to remove the template. After 5 minutes of incubation with EDTA, the particles were centrifuged and recovered. This process was repeated three times to ensure the complete removal of the sacrificial template (Fig. 1). The resulting capsules were washed several times with PBS or distilled water for the following use and characterization.

In a particular case, FITC-labelled PAH was used for the fabrication of fluorescently-labelled capsules to analyse the internalization of the polymer capsules by the cells. To do so, PAH and FITC were mixed at a ratio of 100 mol amide group of PAH per 1 mol of FITC. Briefly, PAH was dissolved in a 500 mM carbonate buffer (pH = 9.5) and then FITC solution (1 mg/mL in DMSO) was added dropwise to this solution sheltered from light. After 30 min of incubation, the solution was dialyzed for 48 h against distilled water, using a dialysis tubing cellulose membrane (avg. flat with 10 mm) (Sigma Aldrich). Once the dialysis process finished, the solution was freeze-dried (Telstar LyoQuest).

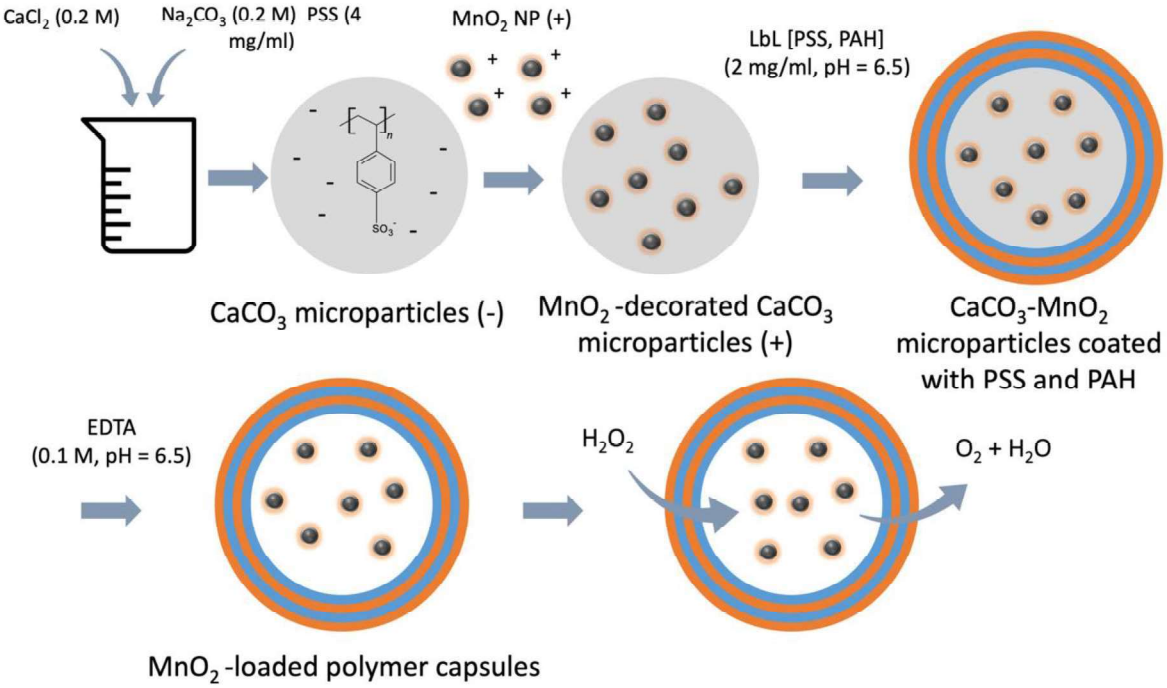

Figure 1. Schematic representation of the fabrication of MnO_2-loaded antioxidant polymer capsules.

2.3.2. Physico-chemical and morphological characterization

The morphological analysis of the $CaCO_3$ microparticles and polymer capsules was carried out by means of Scanning Electron Microscopy (SEM: Hitachi S-4800) at a working voltage and working current of 5 kV and 2 nA, respectively.

To confirm the presence of MnO_2 nanoparticles in the $CaCO_3$ microparticles, X-ray Diffraction (XRD) analysis was performed using a PHILIPS X`PERT PRO automatic diffractometer operating at 40 kV and 40 mA, in theta-theta configuration, secondary monochromator with Cu-Kα radiation (λ = 1.5418 Å) and a PIXcel solid state detector.

The size distribution of the $CaCO_3$ microparticles was obtained in a Laser Scattering Particle Size Distribution Analyzer (HORIBA LA-350).

The ζ-potential of the particles after each polyelectrolyte deposition was measured from a minimum of ten runs using a Malvern Instrument Zetasizer (ZEN 3690).

Infrared spectra of the polyelectrolytes and capsules before and after the $CaCO_3$ sacrificial template removal was measured using a Nicolet AVATAR 370 operating in the Attenuated Total Reflectance (ATR-FTIR). Spectra were taken with a resolution of 2 cm^{-1} and averaged over 64 scans.

The complete removal of the template was further confirmed via energy dispersive X-ray spectroscopy (EDS) using a FEI 200 SEM with a built-in Bruker Nano XFlash 5010 detector. The voltage was set at 20 kV and the scanning time at one minute. All the samples were coated with gold at 25 mA for 70 s before analysis.

The antioxidant capacity of the polymer capsules in the presence of biologically relevant H_2O_2 concentration (i.e., 10 µM and 50 µM) was evaluated using a Fluorimetric Hydrogen Peroxide Assay Kit (Sigma Aldrich). Briefly, polymer capsules at a final concentration of $1 \cdot 10^5$, $1 \cdot 10^6$, $1 \cdot 10^7$ or $1 \cdot 10^8$ polymer capsules/mL were incubated in a 10 or 50 µM H_2O_2 solution for 30 min. Afterwards, the dispersion of polymer capsules was centrifuged and 50 µL of the supernatant was transferred to a well in a 96-well plate together with another 50 µL of master mix containing horseradish peroxidase and red peroxidase substrate. After incubating for 20 min sheltered from light, the fluorescence intensity was measured (λ_{ex}=540 nm/λ_{em}=590 nm) on a microplate reader (BioTek Synergy H1M) to determine the H_2O_2 concentration.

The capacity of the capsules to scavenge H_2O_2 capsules after being exposed to several cycles of H_2O_2 was also evaluated. For this purpose, polymer capsules at a final concentration of $1 \cdot 10^8$ capsules/mL were incubated in a 10 or 50 µM H_2O_2 solution for 30 min and subsequently centrifuged. The supernatant was collected to determine the H_2O_2 concentration following the procedure described above (Cycle 1). The polymer capsules were then resuspended in H_2O_2 solution (10 or 50 µM) and incubated for another 30 min. After being centrifuged, the supernatant was collected to determine the H_2O_2 concentration (Cycle 2). This process was repeated until cycle 4.

The H_2O_2 scavenging capacity of the polymer capsules after being sterilized with ethanol was also determined. Here, polymer capsules at a final concentration of $1 \cdot 10^7$ or $1 \cdot 10^8$ polymer capsules/mL were incubated in a 10 µM H_2O_2 solution for 30 min and subsequently centrifuged. The supernatant was collected to determine the H_2O_2 concentration following the procedure described above (non-sterilized sample). The polymer capsules were then resuspended in ethanol for 10 min. They were then collected by centrifugation and incubated in a 10 µM H_2O_2 solution for 30 min. The supernatant was finally collected after centrifugation to determine the H_2O_2 concentration (sterilized sample).

2.4. In vitro studies

2.4.1. HeLa cell seeding

HeLa cells (ATCC) were grown in T-75 flasks with complete medium (DMEM + 10% FBS + 1% P/S) and incubated at 37 °C in a 5% CO_2 atmosphere. For the metabolic activity measurement and H_2O_2 scavenging analysis, the cells were seeded at a density of 50,000 or 5,000 cells/well on a 24 or 96-well plate, respectively.

2.4.2. Preliminary cytocompatibility test

To evaluate the cytotoxicity of the capsules, the metabolic activity of HeLa cells in the presence of polymer capsules was measured using the AlamarBlue® assay. Cells were seeded in 24-well plates and treated with MnO_2-loaded capsules with different surface charge (positive or negative) at three different capsules-to-cell ratios (10, 100 and 1000 polymer capsules/cell). Cells cultured in the absence of capsules were used as a control. At the selected time points (24 h or 72 h), the culture media was removed and replaced by fresh complete media containing AlamarBlue® (10% v/v). Cells were then incubated for 75 min at 37 °C in 5% CO_2 atmosphere sheltered from light. Finally, 200 µL of the assay media was transferred to a 96-well plate and the fluorescence intensity (λ_{ex}=545 nm/λ_{em}=590 nm) was read on a microplate reader (BioTek Synergy H1M).

The internalization of the FITC-labelled capsules by the cells was also analysed. After 24 h incubation of the cells in the presence of polymer capsules (10 capsules/cell), the culture media was removed and the cells were washed with HBSS and fixed with 4% paraformaldehyde. Cells were then washed with HBSS and permeabilized with 0.5% Triton X-100 in PBS for 10 minutes. After that, the cells were washed twice with PBS and incubated in a 1% BSA solution in PBS in the presence of rhodamine-phalloidin (0.066 µM) and DAPI (300 nM) for 15 minutes. Finally, cells were washed twice with PBS-T (0.1% Tween 20) and once with PBS before being observed in an inverted fluorescence microscope (Nikon Eclipse Ts2).

2.4.3. Therapeutic potential of the polymer capsules in a H_2O_2-induced in vitro model

To evaluate the capacity of the capsules to protect cells in a H_2O_2-induced oxidative stress model, cells were first seeded at a concentration of 5,000 cells/well in a 96-well plate in

complete medium. After cell adhesion (4 hours), polymer capsules with either positive or negative surface charge were added at a final ratio of 10, 100 and 1000 capsules/cell and incubated overnight. After this incubation, three stimuli of a biologically relevant H_2O_2 concentration (100 μM) were applied at different time points (0 h, 12 h, 24 h). The metabolic activity was measured using AlamarBlue® assay at the selected time points (8 h, 24 h, 32 h from the first stimulus addition) as described above.

2.5. Statistical analysis

All quantitative data related to the fabrication and characterization of polymer capsules are presented as the mean ± standard deviation (SD). For the *in vitro* studies six technical replicates (n=6) were employed and the results are presented as the mean ± standard deviation (SD). The statistical difference between groups was tested by one-way analysis of variance (ANOVA), using the Bonferroni post-hoc test and a confidence level of 95% ($p<0.05$).

3. Results and discussion

3.1. Synthesis of MnO_2 nanoparticles

Following the experimental procedure described above, we were able to acquire MnO_2 nanoparticles of spherical morphology and an average size of ~50 nm (Fig. 2a, 2b). The FTIR spectrum presented in Fig. 2c shows the characteristic peaks resulting from the PAH-stabilized MnO_2 nanoparticles. More specifically, the peaks in the range of 550-650 cm^{-1} can be attributed to the stretching vibration of Mn-O. Shifting to higher wavenumbers, the stretching vibration of C-H of the PAH coating can be seen in the range of 1435-1485 cm^{-1}, while the asymmetric vibration of N-H can be observed in the range of 1570-1650 cm^{-1}. Finally, the broad peaks in the range of 2800-3000 cm^{-1} and 3140-3400 cm^{-1} are respectively attributed to

the symmetric stretching vibrations of O-H and N-H. Dynamic light scattering measurements were performed to assess the colloidal stability of the synthesized nanoparticles. The results presented in Fig. 2d and 2e show respectively the Gaussian distributions of the hydrodynamic diameter (average size: 129.7 ± 5.1 nm) and of the surface charge (average ζ-potential: +42.4 ± 0.05 mV). The higher hydrodynamic diameter deriving from the DLS measurements can be attributed to the PAH-coating. This coating is also responsible for the positive surface charge as well as the polydispersity (PDI) value of 0.35 ± 0.04. This PDI value suggests a moderate nanoparticle dispersion which can be attributed to the hydrogen bonds that are created between the PAH and the water molecules, affecting the hydrodynamic diameter. However, the strong positive surface charge that indicates strong repulsive electrostatic interactions, as well as the small size of nanoparticles suggest an increased colloidal stability.

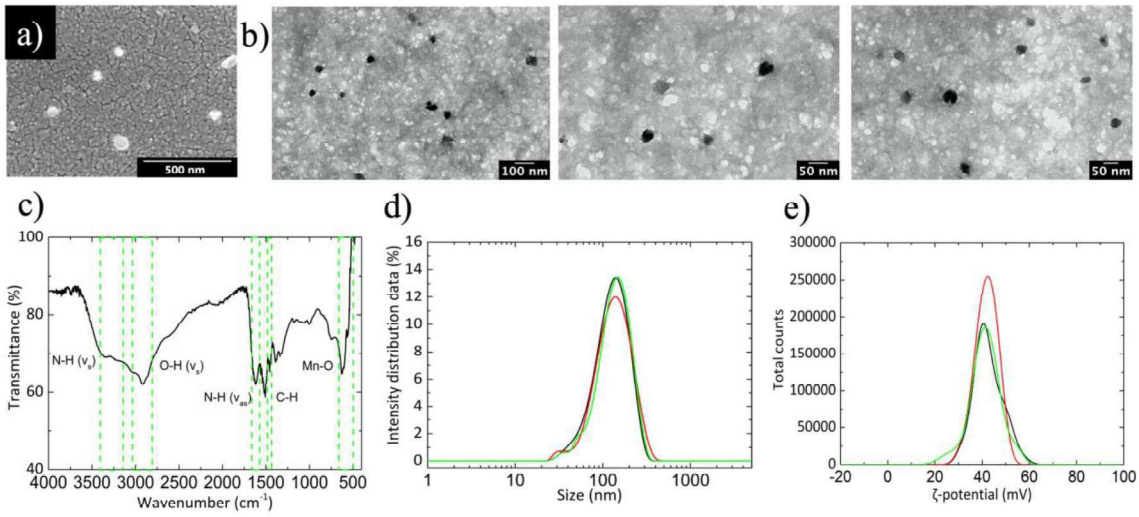

Figure 2. a) Scanning electron micrograph depicting the morphology and size of the synthesized MnO_2 nanoparticles, b) Transmission electron micrograph depicting the morphology and size of the synthesized MnO_2 nanoparticles, c) FTIR spectrum presenting the characteristic peaks of the synthesized nanoparticles, d) size and e) ζ-potential (surface charge) distributions of the synthesized nanoparticles, respectively.

3.2. Fabrication of MnO_2-decorated $CaCO_3$ template

For the fabrication of $CaCO_3$ sacrificial template, $CaCl_2$ and Na_2CO_3 salts were mixed in the presence of PSS. The process resulted in vaterite-like spherical particles with a porous surface and a slightly uniform size distribution (Fig. 3a and 3b). The obtained microparticles had a mean diameter size of 2.73 ± 1.0 µm (Fig. 3f). The addition of PSS plays a pivotal role in the fabrication of the $CaCO_3$ sacrificial template, preventing the recrystallization of the microparticles to calcite-like structure [29] and endowing this $CaCO_3$ template with stability. Furthermore, PSS helps in the achievement of a narrower particle diameter distribution and a strong negative surface charge, which would improve the subsequent incorporation of positively charged MnO_2 nanoparticles through electrostatic interactions. Although alternative templates (e.g., polystyrene beads, silica nanoparticles) could yield smaller particles with a narrower distribution of sizes, the use of $CaCO_3$ microparticles brings the opportunity to fabricate capsules by using mild conditions (i.e., avoiding the use of organic solvents and/or extremely acidic/basic conditions for core removal). This is vital to preserve the integrity of the assembled layers. Great efforts are being made to improve the polydispersity of $CaCO_3$-based templates by using, among others, PSS, ethylene glycol (EG) or glycerol as additional reagents in the precipitation reaction [30–33].

After the incubation process of the $CaCO_3$ sacrificial templates with the MnO_2 nanoparticles, particles of 2.99 ± 1.1 µm (Fig. 3g) were obtained. No significant differences were observed in size distribution and morphology between the MnO_2-decorated $CaCO_3$ templates and non-decorated templates (Fig. 3a-3d). The successful incorporation of MnO_2 in the sacrificial template was confirmed by XRD analysis, where diffraction peaks at 19º and 38º associated to MnO_2 appeared in the diffractogram (Fig. 3e). As the adsorbed MnO_2 quantity will affect the

H_2O_2 scavenging capacity, the ratio 4 mg MnO_2: 10 mg $CaCO_3$ microparticles was chosen to maximize the adsorbed MnO_2 quantity. To optimize this ratio, $CaCO_3$ microparticles were incubated with different amounts of MnO_2 nanoparticles (e.g., 2, 4, 8 and 10 mg of MnO_2 with 10 mg of $CaCO_3$ microparticles) and after the dissolution of the template with EDTA a similar MnO_2 adsorption was observed at all the studied ratios (Fig S1), suggesting that an excess of MnO_2 that ensures maximum MnO_2 adsorption was employed in all the cases.

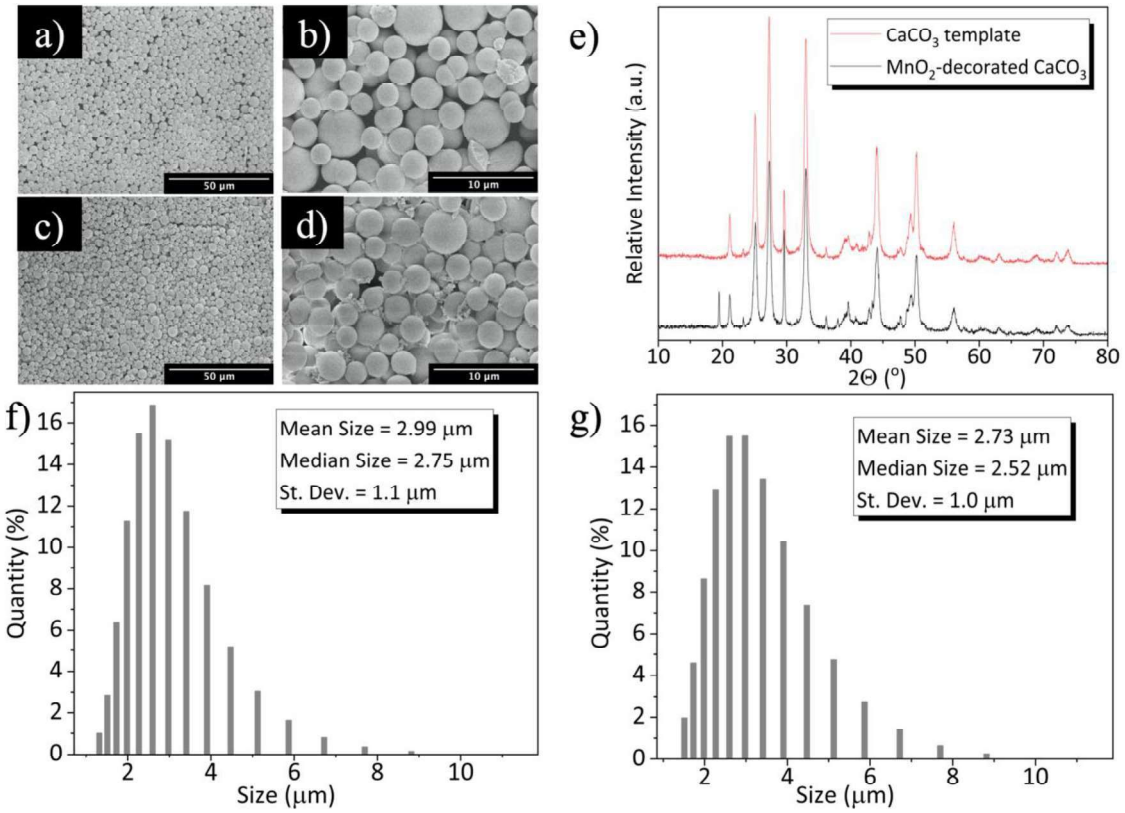

Figure 3. Morphological characterization via SEM (a-d) of $CaCO_3$ templates (a and b) and MnO_2-decorated $CaCO_3$ templates (c and d). e) XRD spectra of the sacrificial template. f) Size distribution of $CaCO_3$ microparticles and MnO_2-decorated $CaCO_3$ microparticles.

3.3. Fabrication of polymer capsules via the layer-by-layer approach

For the fabrication of polymer capsules, positively charged PAH and negatively charged PSS were deposited alternately onto $CaCO_3$ cores. These polyelectrolytes were chosen for the formation of the shell, due to their active use, as model polyelectrolytes, in the fabrication of different therapeutic systems [34–37]. In the development of advanced materials for biomedical applications, the use of biodegradable polymers such as chitosan and alginate are highly desirable. However, for the particular application of polymer capsules as nano- and microreactors, a fast degradation of the polymeric shell could be detrimental. Therefore, a timely degradation of the polymer capsule while ensuring the diffusion of reagents and by-products through the polymeric shell should be ensured, which can be achieved by the precise control of the crosslinking degree.

The initial surface charge of the $CaCO_3$ template was positive in the case of MnO_2-decorated sacrificial templates, whereas it was negative in the non-decorated templates. MnO_2-decorated $CaCO_3$ microparticles were first incubated with PSS and the surface charge shifted from +5.0 mV to -21.5 mV (Fig. 4c). In the case of $CaCO_3$ microparticles without MnO_2, the first layer was made of PAH and the ζ–potential value changed from -17.7 mV to -1.7 mV (Fig. 4c). Thereafter, polyelectrolyte layers were assembled alternately and a sequential charge reversal was observed in the ζ–potential, demonstrating the successful assembly of the layers (Fig. 4c).

After the LbL process, the $CaCO_3$ sacrificial template was removed by the immersion of the microparticles in 0.1 M EDTA. As observed by SEM (Fig. 4a and 4b), after the EDTA incubation, the capsules were hollow, owing to their collapsed shape. To confirm the complete removal of the sacrificial template, FTIR and EDS spectra were acquired. In the FTIR spectra

(Fig. 4f), the two main bands of the $CaCO_3$ at 1384 cm^{-1} and 870 cm^{-1} were observed before the EDTA immersion. After the EDTA addition, these bands disappeared and only the characteristic bands of PAH and PSS were detected. In the EDS (Fig. 4d and 4e), no traces of calcium were observed in the spectrum after the EDTA addition, confirming the complete removal of the template.

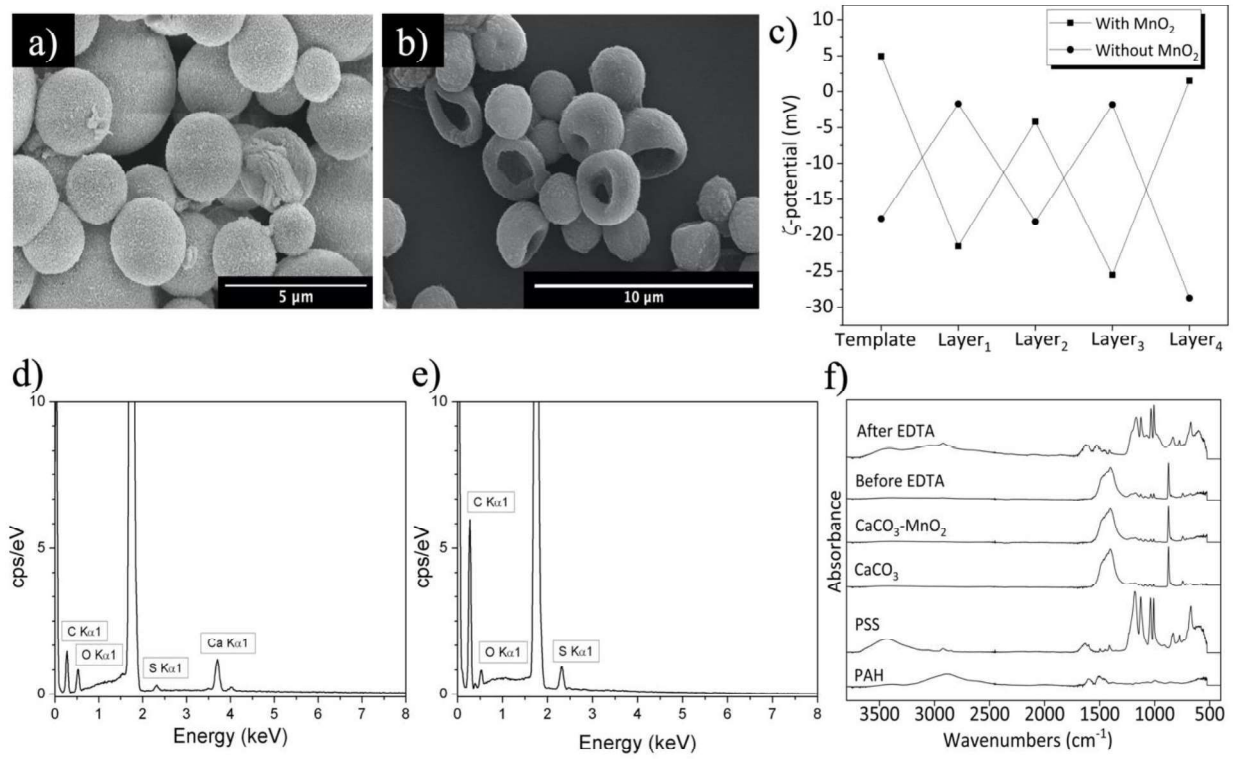

Figure 4. Morphological characterization via SEM (a and b) of polymer capsules a) before and b) after 0.1 M EDTA addition. c) ζ–potential of $CaCO_3$ microparticles and MnO_2-decorated microparticles after each polyelectrolyte deposition. EDS spectra of polymer capsules d) before and e) after 0.1 M EDTA addition. f) FTIR spectra of polymer capsules before and after 0.1 M EDTA addition.

The resulting hollow polymer capsules were incubated with two biologically relevant H_2O_2 concentrations (10 µM and 50 µM) at a final concentration of $1{\cdot}10^5$, $1{\cdot}10^6$, $1{\cdot}10^7$, $1{\cdot}10^8$ polymer capsules/mL for 30 min to assess their antioxidant capacity. At the 50 µM H_2O_2

concentration, a significant ($p<0.05$) decrease in the H_2O_2 concentration was observed only in the case of $1 \cdot 10^8$ capsules/mL (from 100 ± 6% to 45 ± 3%) (Fig. 5a). At the 10 µM H_2O_2 concentration, significant decreases ($p<0.05$) in the H_2O_2 concentration were observed with the concentrations of $1 \cdot 10^6$, $1 \cdot 10^7$ and $1 \cdot 10^8$ polymer capsules/mL, from the initial value of 100 ± 6% to 84 ± 4%, 64 ± 2% and 6 ± 1%, respectively (Fig. 5a). Taken together, these results confirm the H_2O_2 scavenging capacity of the developed capsules. The reaction between the MnO_2 nanoparticles embedded in the polymer capsules and H_2O_2 results in the generation of O_2 as previously reported by us and others [1,3,38–40].

To test the regeneration capacity of the capsules to scavenge H_2O_2, capsules were subjected to several H_2O_2 scavenging cycles. Capsules were incubated with two different H_2O_2 concentrations (10 and 50 µM) in four subsequent cycles at a concentration of $1 \cdot 10^8$ capsules/mL. The supernatant of each incubation was collected to analyse the H_2O_2 reduction capacity (Fig. 5b), considering 100% reduction capacity the reduction observed in the first cycle. In both cases, a significant decrease ($p<0.05$) of the H_2O_2 scavenging capacity was observed after the second cycle. However, the capsules were able to maintain a 34 ± 6% and 58 ± 1% of their activity after the fourth cycle for the H_2O_2 concentrations of 50 and 10 µM, respectively.

To analyse the effect of sterilization on the scavenging capacity, the capsules were sterilized with ethanol and subsequently incubated with 10 µM H_2O_2 at different concentrations ($1 \cdot 10^7$ and $1 \cdot 10^8$ polymer capsules/mL). In the case of $1 \cdot 10^7$ capsules/mL, there was a significant decrease ($p<0.05$) in the H_2O_2 scavenging capacity of the sterilized capsules with respect to the non-sterilized ones (Fig. 5c). This can be associated to the reversible reorganization of the polyelectrolytes in the water/ethanol mixture that causes an increased permeability of the shell

and subsequent loss of MnO_2 nanoparticles from the interior of the capsule [41]. Nevertheless, capsules were able to maintain a 69 ± 6% H_2O_2 scavenging capacity after their sterilization with ethanol. At $1 \cdot 10^8$ capsules/mL, no significant change ($p<0.05$) in the scavenging capacity was observed after the sterilization process. Therefore, the stability of the capsules facing different processes is significant and ensures the utility of these capsules in the disease treatment environment and process.

The leakage of MnO_2 nanoparticles was confirmed by incubating polymer capsules in PBS and measuring the concentration of MnO_2 nanoparticles in the supernatant by means of UV-VIS at different time points (i.e., day 1, 2 and 3). It was observed that almost all the loaded MnO_2 (104.6 ± 11.5µg) was released after three days in PBS (Fig S2), suggesting an increased permeability of the polymer shell that contribute to the leakage of the embedded nanoparticles.

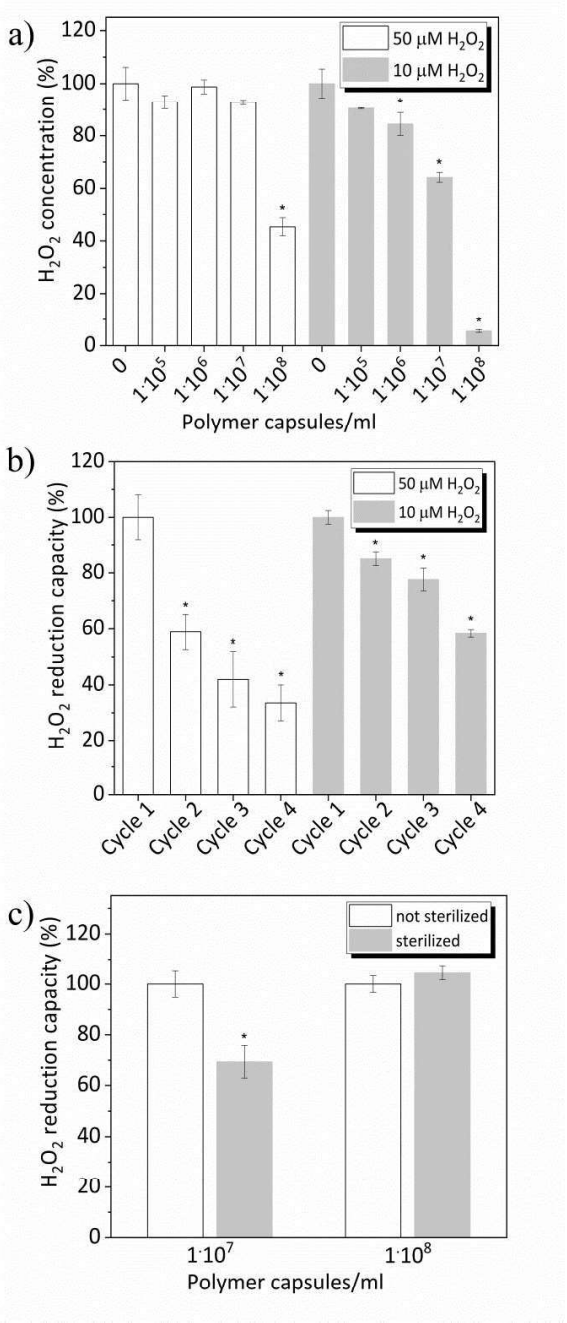

Figure 5. a) H_2O_2 scavenging capacity of the polymer capsules at biologically relevant H_2O_2 concentrations (10 μM and 50 μM). b) H_2O_2 scavenging capacity of the polymer capsules after four H_2O_2 (10 μM and 50 μM) cycles. Capsules were incubated at a concentration of $1 \cdot 10^8$ capsules/mL and it was considered 100% reduction capacity the reduction obtained in the first cycle. c) H_2O_2 scavenging capacity of the polymer capsules at 10 μM H_2O_2 after the sterilization process. Asterisks (*) indicate significant differences ($p<0.05$) with respect to each control (0 capsules/mL in (a), cycle 1 in (b), non-sterilized capsules in (c)).

3.4. Metabolic activity of HeLa cells in the presence of capsules and capsule internalization

To evaluate the *in vitro* cytocompatibility of the developed capsules, either positively (i.e., PSS-PAH-PSS-PAH) or negatively charged (PSS-PAH-PSS-PAH-PSS) capsules were incubated with HeLa cells at different capsule per cell ratios (10, 100, 1000 capsules/cell) and the metabolic activity of cells was measured after one and three days by means of AlamarBlue® assay. In the case of positively charged capsules, a significant decrease ($p<0.05$) in the metabolic activity of cells was observed after one day of incubation at all the studied ratios (Fig. 6a). Note that the metabolic activity was below the threshold value (i.e., 70%) in the cases of 100 and 1000 capsules/cell. In contrast, cells were able to maintain higher metabolic activities in the presence of negatively charged capsules and, in this case, the metabolic activity of the cells was above 79 ± 7 % in all the cases (Fig. 6a).

At day three, no significant differences ($p<0.05$) were observed in the metabolic activity of cells in the presence of 10 capsules/cell with respect to the control (i.e., in the absence of capsules). The metabolic activity of cells was below the threshold value (i.e., 70 %) at 100 and 1000 capsules/cell in the case of positively charged capsules. In contrast, cells were able to maintain a metabolic activity >81 ± 5 % at 100 capsules/cell in the case of negatively charged capsules and only in the case of 1000 capsules/cell the metabolic activity was below the threshold value (i.e., 70%). Taken together, the results indicate a lower cytotoxicity of the negatively charged capsules with respect to the positively charged ones. Regarding the Mn^{2+} production after the reaction with H_2O_2, it has been reported that an excessive and chronic exposure to high concentrations and the accumulation of manganese can lead to neurotoxicity and irreversible brain disease [40,42–44]. Despite this controversial effects, other studies suggest that Mn^{2+} ions can be physically metabolized without a long retention in the body and

any toxic effect [28,45,46]. Furthermore, as demonstrated by the cytotoxic evaluation, the amount of manganese used in this work (5.2 µg/well) is not enough to induce any cytotoxic effect.

To determine the uptake and distribution of the capsules in the cellular microenvironment, polymer capsules were observed under optical and fluorescence microscope. As observed in Fig. 6b, negatively charged capsules were uniformly distributed and few capsules were attached to the cells. In contrast, positively charged capsules were accumulated generally around the cells (Fig. 6c). For the fluorescence microscope analysis, capsules were fabricated using FITC-labelled PAH. Fig. 6d and 6e show the internalization of the negatively and positively charged capsules, respectively. In both cases, few capsules were localized in the cytoplasm and showed a collapsed shape, whereas some other capsules were observed around the cell membrane retaining their spherical shape. Based on the micrographs obtained with the fluorescent microscope, the differences between positively and negatively charged polymer capsules were not relevant.

The obtained results in the metabolic activity analysis and the internalization and distribution demonstrate that, as reported in bibliography, positively charged capsules are preferably taken up or attached to the cells but they induce a higher cytotoxic response [50]. The cytoplasmic membrane of cells is typically negatively charged. Consequently, positively charged capsules display a higher cellular binding as it is observed in the obtained results [51,52]. As observed in the fluorescent micrographs, most of the capsules were accumulated preferably around the cellular membrane and low internalization was observed. Based on these results, we believe that the polymer capsules developed in this work primarily reduce the ROS from the extracellular microenvironment. The uptake of the capsules for an efficient reduction of

intracellular ROS could be promoted by using either smaller capsules or surface functionalization strategies [47–49].

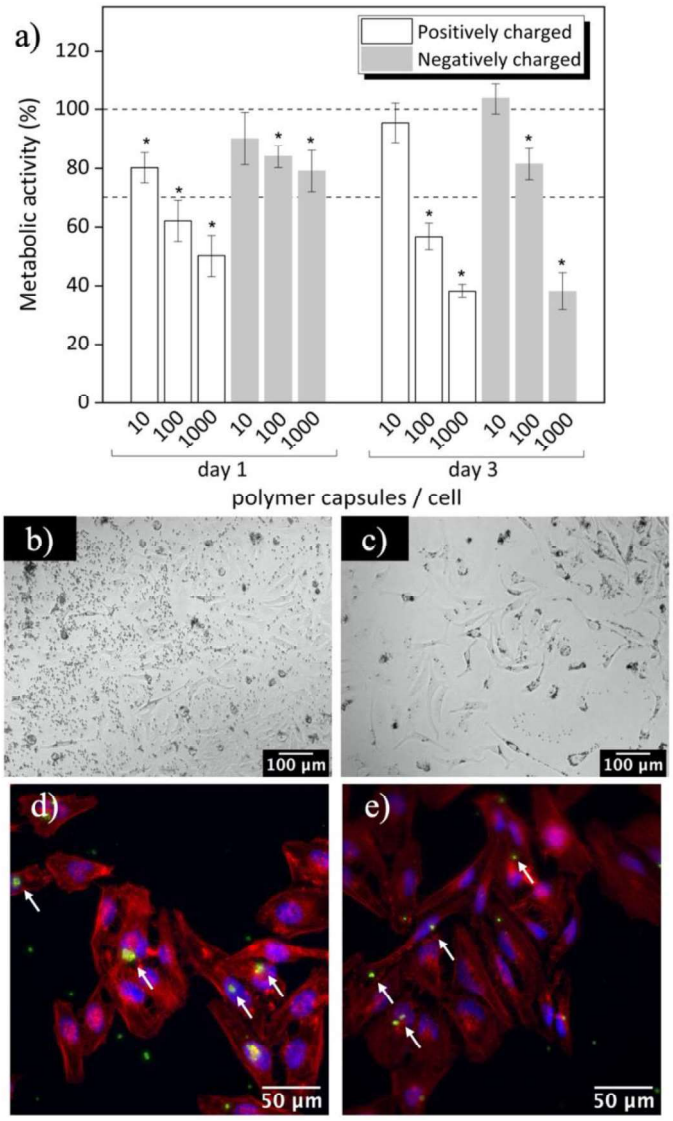

Figure 6. a) Metabolic activity of HeLa cells in the presence of polymer capsules. Asterisks (*) indicate significant differences ($p<0.05$) with respect to the control (0 capsules/mL). Distribution of b) negatively and c) positively charged polymer capsules in the cellular microenvironment. Fluorescent micrographs of HeLa cells in the presence of d) negatively and e) positively charged polymer capsules (Nuclei-DAPI: Blue / Cytoplasm-Rhodamine Phalloidin: Red / Polymer capsules-FITC: Green). White arrows highlight the presence of FITC-labelled polymer capsules.

3.5. Therapeutic potential of the polymer capsules in a H_2O_2-induced oxidative stress in vitro model

The therapeutic potential of the polymer capsules was evaluated in a H_2O_2-induced *in vitro* model with positively and negatively charged capsules. In this model, 100 μM H_2O_2 stimuli were added every 12 hours to the cells to induce oxidative stress. Metabolic activity of the cells was measured by the AlamarBlue® assay at the selected time points (8, 24 and 32 h after the first stimulus). The concentration of the H_2O_2 stimuli (100 μM) was chosen after an analysis of different H_2O_2 concentrations (data not shown) to ensure an extreme situation which can cause cell death and/or significant reduction in the observed metabolic activity. As a negative control, HeLa cells were cultured in the absence of capsules and H_2O_2 stimuli. As a positive control, HeLa cells in the absence of capsules but with 100 μM H_2O_2 stimuli were used.

As expected from the previously performed *in vitro* cytocompatibility test (Fig. 6a), the positively charged capsules had a detrimental effect on the metabolic activity of cells at the higher ratios (i.e., 100 and 1000 capsules/cell), thus limiting their therapeutic potential. The metabolic activity of the cells at 8 h and 24 h in the presence of capsules was not significantly different ($p<0.05$) with respect to the controls, with the exception of the positively charged capsules at the concentrations of 100 and 1000 capsules/cell and negatively charged capsules at the concentration of 1000 capsules/cell. In these cases, a significant decrease ($p<0.05$) in the metabolic activity was observed with respect to the negative control.

At 24 h, a significant difference ($p<0.05$) was observed between the positive and negative control, which became larger at 32 h due to the induced oxidative stress. Interestingly, the addition of positively charged capsules at a concentration of 10 capsules/cell and negatively

charged capsules at a concentration of 10 or 100 capsules/cell resulted in a significant increase ($p<0.05$) in the metabolic activity with respect to the positive control, thus suggesting a protective effect towards oxidative stress. In view of these results, to obtain an efficient therapeutic effect against the overproduction of H_2O_2, both the concentration and surface charge of the capsules should be carefully considered.

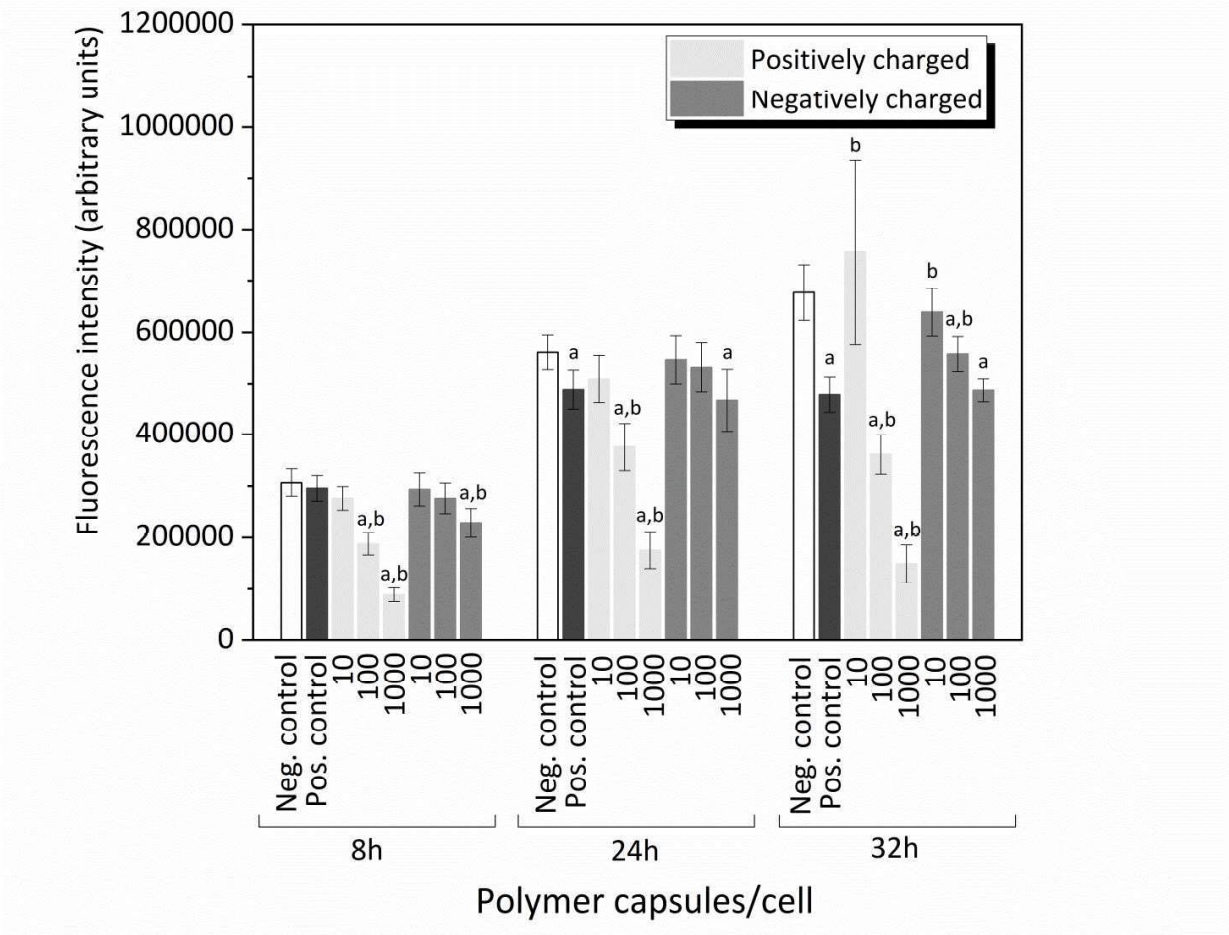

Figure 7. Metabolic activity of HeLa cells in the presence of H_2O_2 stimuli (100 μM) and polymer capsules. The "a" and "b" indicate significant differences ($p<0.05$) with respect to the negative (cells in the absence of capsules and H_2O_2) and the positive control (cells in the absence of capsules but with the addition of H_2O_2), respectively (n=6).

4. Conclusions

In the present work, we fabricated MnO_2-loaded polymer capsules via the LbL approach. The developed capsules acted as antioxidant microreactors and were able to reduce H_2O_2 from solution at biologically relevant concentrations. The capsules were robust, as demonstrated by their capacity to scavenge H_2O_2 from solution after several cycles and after being sterilized with ethanol. The stability towards ethanol sterilization is of particular interest for the potential use of these capsules in biomedical applications. The cytocompatibility of the developed capsules was assessed *in vitro*, where significant differences between the positively and negatively charged capsules were observed. Positively charged capsules were accumulated around the cells and caused a detrimental effect on their metabolic activity at the higher concentrations (100 and 1000 capsules/cell), thus limiting their therapeutic potential. In contrast, negatively charged capsules were uniformly distributed in the cellular microenvironment and preserved the metabolic activity of cells better. In the developed H_2O_2-induced oxidative stress model, some beneficial response was observed for the concentration of 10 capsules/cell in positively charged capsules and for 10 and 100 capsules/cell in negatively charged capsules. This study represents a novel strategy for the fabrication of antioxidant polymer microreactors, where the traditional encapsulation of antioxidant enzymes has been replaced by manganese dioxide nanoparticles, thus providing a more robust and stable inorganic alternative.

Acknowledgments

The authors are thankful for funds from the Basque Government, Department of Education (IT-927-16). SGIker technical services (UPV/EHU) are gratefully acknowledged for XRD and SEM support.

References

[1] C. Tapeinos, A. Larrañaga, J.R. Sarasua, A. Pandit, Functionalised collagen spheres reduce H2O2 mediated apoptosis by scavenging overexpressed ROS, Nanomedicine Nanotechnology, Biol. Med. 14 (2018) 2397–2405. doi:10.1016/j.nano.2017.03.022.

[2] C. De Gracia Lux, S. Joshi-Barr, T. Nguyen, E. Mahmoud, E. Schopf, N. Fomina, A. Almutairi, Biocompatible polymeric nanoparticles degrade and release cargo in response to biologically relevant levels of hydrogen peroxide, J. Am. Chem. Soc. 134 (2012) 15758–15764. doi:10.1021/ja303372u.

[3] D.R. Pereira, C. Tapeinos, A.L. Rebelo, J.M. Oliveira, R.L. Reis, A. Pandit, Scavenging Nanoreactors that Modulate Inflammation, Adv. Biosyst. 2 (2018) 1–13. doi:10.1002/adbi.201800086.

[4] G.C. Van De Bittner, E.A. Dubikovskaya, C.R. Bertozzi, C.J. Chang, In vivo imaging of hydrogen peroxide production in a murine tumor model with a chemoselective bioluminescent reporter, Proc. Natl. Acad. Sci. U. S. A. 107 (2010) 21316–21321. doi:10.1073/pnas.1012864107.

[5] A. Larrañaga, M. Lomora, J.R. Sarasua, C.G. Palivan, A. Pandit, Polymer capsules as micro-/nanoreactors for therapeutic applications: Current strategies to control membrane permeability, Prog. Mater. Sci. 90 (2017) 325–357. doi:10.1016/j.pmatsci.2017.08.002.

[6] S. Donatan, A. Yashchenok, N. Khan, B. Parakhonskiy, M. Cocquyt, B. El Pinchasik, D. Khalenkow, H. Möhwald, M. Konrad, A. Skirtach, Loading Capacity versus Enzyme Activity in Anisotropic and Spherical Calcium Carbonate Microparticles, ACS Appl.

Mater. Interfaces. 8 (2016) 14284–14292. doi:10.1021/acsami.6b03492.

[7] Y. Ping, J. Guo, H. Ejima, X. Chen, J.J. Richardson, H. Sun, F. Caruso, PH-Responsive capsules engineered from metal-phenolic networks for anticancer drug delivery, Small. 11 (2015) 2032–2036. doi:10.1002/smll.201403343.

[8] G. Schneider, G. Decher, Functional core/shell nanoparticles via layer-by-layer assembly. Investigation of the experimental parameters for controlling particle aggregation and for enhancing dispersion stability, Langmuir. 24 (2008) 1778–1789. doi:10.1021/la7021837.

[9] N. Boehnke, S. Correa, L. Hao, W. Wang, J.P. Straehla, S.N. Bhatia, P.T. Hammond, Theranostic Layer-by-Layer Nanoparticles for Simultaneous Tumor Detection and Gene Silencing, Angew. Chemie - Int. Ed. 02115 (2020) 2–10. doi:10.1002/anie.201911762.

[10] A.S. Timin, A.R. Muslimov, M. V. Zyuzin, O.O. Peltek, T.E. Karpov, I.S. Sergeev, A.I. Dotsenko, A.A. Goncharenko, N.D. Yolshin, A. Sinelnik, B. Krause, T. Baumbach, M.A. Surmeneva, R. V. Chernozem, G.B. Sukhorukov, R.A. Surmenev, Multifunctional Scaffolds with Improved Antimicrobial Properties and Osteogenicity Based on Piezoelectric Electrospun Fibers Decorated with Bioactive Composite Microcapsules, ACS Appl. Mater. Interfaces. 10 (2018) 34849–34868. doi:10.1021/acsami.8b09810.

[11] D. Valdepérez, P. del Pino, L. Sánchez, W.J. Parak, B. Pelaz, Highly active antibody-modified magnetic polyelectrolyte capsules, J. Colloid Interface Sci. 474 (2016) 1–8. doi:10.1016/j.jcis.2016.04.003.

[12] H. Gao, D. Wen, N. V. Tarakina, J. Liang, A.J. Bushby, G.B. Sukhorukov, Bifunctional

ultraviolet/ultrasound responsive composite TiO2/polyelectrolyte microcapsules, Nanoscale. 8 (2016) 5170–5180. doi:10.1039/c5nr06666b.

[13] D.A. Gorin, S.A. Portnov, O.A. Inozemtseva, Z. Luklinska, A.M. Yashchenok, A.M. Pavlov, A.G. Skirtach, H. Möhwald, G.B. Sukhorukov, Magnetic/gold nanoparticle functionalized biocompatible microcapsules with sensitivity to laser irradiation, Phys. Chem. Chem. Phys. 10 (2008) 6899–6905. doi:10.1039/b809696a.

[14] A.M. Pavlov, V. Saez, A. Cobley, J. Graves, G.B. Sukhorukov, T.J. Mason, Controlled protein release from microcapsules with composite shells using high frequency ultrasound - Potential for in vivo medical use, Soft Matter. 7 (2011) 4341–4347. doi:10.1039/c0sm01536a.

[15] A.S. Timin, A.R. Muslimov, K. V. Lepik, O.S. Epifanovskaya, A.I. Shakirova, U. Mock, K. Riecken, M. V. Okilova, V.S. Sergeev, B. V. Afanasyev, B. Fehse, G.B. Sukhorukov, Efficient gene editing via non-viral delivery of CRISPR–Cas9 system using polymeric and hybrid microcarriers, Nanomedicine Nanotechnology, Biol. Med. 14 (2018) 97–108. doi:10.1016/j.nano.2017.09.001.

[16] A.S. Timin, A.R. Muslimov, K. V. Lepik, M. V. Okilova, N.Y. Tcvetkov, A.I. Shakirova, B. V. Afanasyev, D.A. Gorin, G.B. Sukhorukov, Intracellular Breakable and Ultrasound-Responsive Hybrid Microsized Containers for Selective Drug Release into Cancerous Cells, Part. Part. Syst. Charact. 34 (2017) 1–10. doi:10.1002/ppsc.201600417.

[17] D. V. Voronin, O.A. Sindeeva, M.A. Kurochkin, O. Mayorova, I. V. Fedosov, O. Semyachkina-Glushkovskaya, D.A. Gorin, V. V. Tuchin, G.B. Sukhorukov, In Vitro

and in Vivo Visualization and Trapping of Fluorescent Magnetic Microcapsules in a Bloodstream, ACS Appl. Mater. Interfaces. 9 (2017) 6885–6893. doi:10.1021/acsami.6b15811.

[18] S. V. German, D.N. Bratashov, N.A. Navolokin, A.A. Kozlova, M. V. Lomova, M. V. Novoselova, E.A. Burilova, V. V. Zyev, B.N. Khlebtsov, A.B. Bucharskaya, G.S. Terentyuk, R.R. Amirov, G.N. Maslyakova, G.B. Sukhorukov, D.A. Gorin, In vitro and in vivo MRI visualization of nanocomposite biodegradable microcapsules with tunable contrast, Phys. Chem. Chem. Phys. 18 (2016) 32238–32246. doi:10.1039/C6CP03895F.

[19] A. Larrañaga, I.L.M. Isa, V. Patil, S. Thamboo, M. Lomora, M.A. Fernández-Yague, J.R. Sarasua, C.G. Palivan, A. Pandit, Antioxidant functionalized polymer capsules to prevent oxidative stress, Acta Biomater. 67 (2018) 21–31. doi:10.1016/j.actbio.2017.12.014.

[20] A.L. Popov, N. Popova, D.J. Gould, A.B. Shcherbakov, G.B. Sukhorukov, V.K. Ivanov, Ceria Nanoparticles-Decorated Microcapsules as a Smart Drug Delivery/Protective System: Protection of Encapsulated P. pyralis Luciferase, ACS Appl. Mater. Interfaces. 10 (2018) 14367–14377. doi:10.1021/acsami.7b19658.

[21] Q. Wang, H. Wei, Z. Zhang, E. Wang, S. Dong, Nanozyme: An emerging alternative to natural enzyme for biosensing and immunoassay, TrAC - Trends Anal. Chem. 105 (2018) 218–224. doi:10.1016/j.trac.2018.05.012.

[22] A.L. Popov, N.R. Popova, N. V. Tarakina, O.S. Ivanova, A.M. Ermakov, V.K. Ivanov, G.B. Sukhorukov, Intracellular Delivery of Antioxidant CeO2 Nanoparticles via Polyelectrolyte Microcapsules, ACS Biomater. Sci. Eng. 4 (2018) 2453–2462.

doi:10.1021/acsbiomaterials.8b00489.

[23] W. Li, Z. Liu, C. Liu, Y. Guan, J. Ren, X. Qu, Manganese Dioxide Nanozymes as Responsive Cytoprotective Shells for Individual Living Cell Encapsulation, Angew. Chemie - Int. Ed. 56 (2017) 13661–13665. doi:10.1002/anie.201706910.

[24] Y.-W. Bao, X.-W. Hua, J. Zeng, F.-G. Wu, Bacterial Template Synthesis of Multifunctional Nanospindles for Glutathione Detection and Enhanced Cancer-Specific Chemo-Chemodynamic Therapy, Research. 2020 (2020) 9301215. doi:10.34133/2020/9301215.

[25] K.F. Xu, H.R. Jia, Y.X. Zhu, X. Liu, G. Gao, Y.H. Li, F.G. Wu, Cholesterol-Modified Dendrimers for Constructing a Tumor Microenvironment-Responsive Drug Delivery System, ACS Biomater. Sci. Eng. 5 (2019) 6072–6081. doi:10.1021/acsbiomaterials.9b01386.

[26] Y. Lin, J. Ren, X. Qu, Catalytically active nanomaterials: A promising candidate for artificial enzymes, Acc. Chem. Res. 47 (2014) 1097–1105. doi:10.1021/ar400250z.

[27] Q. Chen, L. Feng, J. Liu, W. Zhu, Z. Dong, Y. Wu, Z. Liu, Intelligent Albumin–MnO2Nanoparticles as pH-/H2O2-Responsive Dissociable Nanocarriers to Modulate Tumor Hypoxia for Effective Combination Therapy, Adv. Mater. 28 (2016) 7129–7136. doi:10.1002/adma.201601902.

[28] P. Prasad, C.R. Gordijo, A.Z. Abbasi, A. Maeda, A. Ip, M. Rauth, R.S. Dacosta, X.Y. Wu, Multifunctional Albumin À MnO 2 Nanoparticles Modulate Solid Tumor Microenvironment by Attenuating Enhance Radiation Response, (2014) 3202–3212.

doi:10.1021/nn405773r.

[29] C. Wang, C. He, Z. Tong, X. Liu, B. Ren, F. Zeng, Combination of adsorption by porous CaCO3 microparticles and encapsulation by polyelectrolyte multilayer films for sustained drug delivery, Int. J. Pharm. 308 (2006) 160–167. doi:10.1016/j.ijpharm.2005.11.004.

[30] A. Cai, X. Xu, H. Pan, J. Tao, R. Liu, R. Tang, K. Cho, Direct synthesis of hollow vaterite nanospheres from amorphous calcium carbonate nanoparticles via phase transformation, J. Phys. Chem. C. 112 (2008) 11324–11330. doi:10.1021/jp801408k.

[31] S.E. Facchinetto, T. Bortolotto, G.E. Neumann, J.C.B. Vieira, B.B. De Menezes, C. Giacomelli, V. Schmidt, Synthesis of Submicrometer Calcium Carbonate Particles from Inorganic Salts Using Linear Polymers as Crystallization Modifiers, J. Braz. Chem. Soc. 28 (2017) 547–556. doi:10.5935/0103-5053.20160196.

[32] Y. Tarakanchikova, J. Alzubi, V. Pennucci, M. Follo, B. Kochergin, A. Muslimov, I. Skovorodkin, S. Vainio, M.N. Antipina, V. Atkin, A. Popov, I. Meglinski, T. Cathomen, T.I. Cornu, D.A. Gorin, G.B. Sukhorukov, I. Nazarenko, Biodegradable Nanocarriers Resembling Extracellular Vesicles Deliver Genetic Material with the Highest Efficiency to Various Cell Types, Small. (2019). doi:10.1002/smll.201904880.

[33] D.B. Trushina, T. V. Bukreeva, M.N. Antipina, Size-Controlled Synthesis of Vaterite Calcium Carbonate by the Mixing Method: Aiming for Nanosized Particles, Cryst. Growth Des. 16 (2016) 1311–1319. doi:10.1021/acs.cgd.5b01422.

[34] S. Ashraf, A. Taylor, J. Sharkey, M. Barrow, P. Murray, B. Wilm, H. Poptani, M.J.

Rosseinsky, D.J. Adams, R. Lévy, In vivo fate of free and encapsulated iron oxide nanoparticles after injection of labelled stem cells , Nanoscale Adv. 1 (2019) 367–377. doi:10.1039/c8na00098k.

[35] D. Luo, R.N. Poston, D.J. Gould, G.B. Sukhorukov, Magnetically targetable microcapsules display subtle changes in permeability and drug release in response to a biologically compatible low frequency alternating magnetic field, Mater. Sci. Eng. C. 94 (2019) 647–655. doi:10.1016/j.msec.2018.10.031.

[36] C. Guo, J. Wang, Z. Dai, Selective content release from light-responsive microcapsules by tuning the surface plasmon resonance of gold nanorods, Microchim. Acta. 173 (2011) 375–382. doi:10.1007/s00604-011-0570-y.

[37] A.M. Yashchenok, D.N. Bratashov, D.A. Gorin, M. V. Lomova, A.M. Pavlov, A. V. Sapelkin, B.S. Shim, G.B. Khomutov, N.A. Kotov, G.B. Sukhorukov, H. Möhwald, A.G. Skirtach, Carbon nanotubes on polymeric microcapsules: Freestanding structures and point-wise laser openings, Adv. Funct. Mater. 20 (2010) 3136–3142. doi:10.1002/adfm.201000846.

[38] J. Bizeau, C. Tapeinos, C. Marella, A. Larrañaga, A. Pandit, Synthesis and characterization of hyaluronic acid coated manganese dioxide microparticles that act as ROS scavengers, Colloids Surfaces B Biointerfaces. 159 (2017) 30–38. doi:10.1016/j.colsurfb.2017.07.081.

[39] C. Tapeinos, F. Tomatis, M. Battaglini, A. Larrañaga, A. Marino, I.A. Telleria, M. Angelakeris, D. Debellis, F. Drago, F. Brero, P. Arosio, A. Lascialfari, A. Petretto, E. Sinibaldi, G. Ciofani, Cell Membrane-Coated Magnetic Nanocubes with a Homotypic

Targeting Ability Increase Intracellular Temperature due to ROS Scavenging and Act as a Versatile Theranostic System for Glioblastoma Multiforme, Adv. Healthc. Mater. 8 (2019). doi:10.1002/adhm.201900612.

[40] M.R. Smith, J. Fernandes, Y. Go, D.P. Jones, Redox dynamics of manganese as a mitochondrial life-death switch Matthew, Biochem. Biophys. Res. Commun. 482 (2017) 388–398. doi:10.1016/j.bbrc.2016.10.126.Redox.

[41] Y. Lvov, A.A. Antipov, A. Mamedov, H. Möhwald, G.B. Sukhorukov, Urease Encapsulation in Nanoorganized Microshells, Nano Lett. 1 (2001) 125–128. doi:10.1021/nl0100015.

[42] S.H. Reaney, G. Bench, D.R. Smith, Brain accumulation and toxicity of Mn(II) and Mn(III) exposures, Toxicol. Sci. 93 (2006) 114–124. doi:10.1093/toxsci/kfl028.

[43] K.A. Zhang Danhui, Kanthasamy Arthi, Anantharama Vellareddy, Effects of Manganese on Tyrosine Hydroxylase (TH) Activity and TH-phosphorylation in a Dopaminergic Neural Cell Line, Toxicol. Appl. Pharmacol. 254 (2008) 65–71. doi:10.1038/jid.2014.371.

[44] H. Afeseh Ngwa, A. Kanthasamy, Y. Gu, N. Fang, V. Anantharam, A.G. Kanthasamy, Manganese nanoparticle activates mitochondrial dependent apoptotic signaling and autophagy in dopaminergic neuronal cells, Toxicol. Appl. Pharmacol. 256 (2011) 227–240. doi:10.1016/j.taap.2011.07.018.

[45] D.R. Hu, L.J. Chen, Y. Qu, J.R. Peng, B.Y. Chu, K. Shi, Y. Hao, L. Zhong, M.Y. Wang, Z.Y. Qian, Oxygen-generating hybrid polymeric nanoparticles with encapsulated

doxorubicin and chlorin e6 for trimodal imaging-guided combined chemo-photodynamic therapy, Theranostics. 8 (2018) 1558–1574. doi:10.7150/thno.22989.

[46] K. Xu, J. Zhang, W. Xue, H. Tong, W. Zhang, K. Xu, J. Zhang, W. Xue, H. Tong, W. Zhang, Z. Zhao, H. Liu, Albumin-stabilized manganese-based nanocomposites with sensitive tumor microenvironment responsivity and their application for efficient SiRNA delivery in brain tumors, J. Mater. Chem. B. 8 (2020) 1507–1515. doi:10.1039/c9tb02341k.

[47] C. Cortez, E. Tomaskovic-Crook, A.P.R. Johnston, B. Radt, S.H. Cody, A.M. Scott, E.C. Nice, J.K. Heath, F. Caruso, Targeting and uptake of multilayered particles to colorectal cancer cells, Adv. Mater. 18 (2006) 1998–2003. doi:10.1002/adma.200600564.

[48] A. El-Sayed, I.A. Khalil, K. Kogure, S. Futaki, H. Harashima, Octaarginine- and octalysine-modified nanoparticles have different modes of endosomal escape, J. Biol. Chem. 283 (2008) 23450–23461. doi:10.1074/jbc.M709387200.

[49] J. Cui, Y. Ju, Z.H. Houston, J.J. Glass, N.L. Fletcher, S. Alcantara, Q. Dai, C.B. Howard, S.M. Mahler, A.K. Wheatley, R. De Rose, P.T. Brannon, B.M. Paterson, P.S. Donnelly, K.J. Thurecht, F. Caruso, S.J. Kent, Modulating Targeting of Poly(ethylene glycol) Particles to Tumor Cells Using Bispecific Antibodies, Adv. Healthc. Mater. 8 (2019) 1–10. doi:10.1002/adhm.201801607.

[50] E. Fröhlich, The role of surface charge in cellular uptake and cytotoxicity of medical nanoparticles, Int. J. Nanomedicine. 7 (2012) 5577–5591. doi:10.2147/IJN.S36111.

[51] A.P.R. Johnston, G.K. Such, S.L. Ng, F. Caruso, Challenges facing colloidal delivery systems: From synthesis to the clinic, Curr. Opin. Colloid Interface Sci. 16 (2011) 171–181. doi:10.1016/j.cocis.2010.11.003.

[52] M. V. Zyuzin, A.S. Timin, G.B. Sukhorukov, Multilayer Capsules Inside Biological Systems: State-of-the-Art and Open Challenges, Langmuir. 35 (2019) 4747–4762. doi:10.1021/acs.langmuir.8b04280.